

Tetragonality of barium titanate powder for a ceramic capacitor application

Dang-Hyok Yoon*

School of Materials Science and Engineering, Yeungnam University, Gyeongsan 712-749, Korea

Although nano-sized barium titanate powder (BaTiO_3) with a high tetragonality (large c/a) is essential to enhance the volumetric efficiency of multi-layer ceramic capacitors (MLCCs) in industry, the tetragonality diminishes with a decrease in particle size and disappears below a critical particle size. Many researchers have investigated an understanding of the relationship between particle size and the tetragonality of BaTiO_3 and tried to increase this value while maintaining the particle size as small as possible. Recent experimental results, including ours, on critical particle sizes and their tetragonality values of fine BaTiO_3 powders are reviewed in this paper.

Key words: Dielectric properties, BaTiO_3 , Capacitors, Tetragonality.

Introduction

Barium titanate (BaTiO_3) is one of the most widely used ceramic materials in industry due to its excellent dielectric properties. The current market share of capacitor business based on this powder represents 80-90% [1]. With the miniaturization trend of electronic devices, most ceramic capacitors have a multi-layered structure which is known as a multi-layer ceramic chip capacitor (MLCC) since tape casting for the fabrication of thin ceramic sheets was developed by Howatt *et al.* in 1947 [2]. Common electronic devices contain large numbers of MLCCs: a cell phone 250, a laptop 400 and an automobile with over 1,000 [3]. An MLCC has alternating layers of dielectric materials and internal metal electrodes as shown in Fig. 1. Until 1995 most MLCCs were fabricated using expensive inner electrode materials such as palladium (Pd) or palladium-silver alloys (Pd/Ag) [4, 5]. As shown in Fig. 2, the tremendous increase in the price of Pd during the 1990s has accelerated the use of base-metal electrodes (BME) such as nickel (Ni) and copper (Cu) [4-6]. Changing to Ni electrodes reduced the cost of MLCC by 50-80% compared to that with the precious metal electrodes. In order to use base-metal electrodes, however, an MLCC should be sintered under a reducing atmosphere because Ni electrodes are oxidized completely in air.

The capacitance of a MLCC is [7]:

$$C = \epsilon_0 \epsilon_r \frac{NA}{d} \quad (1)$$

where ϵ_0 is the absolute permittivity of a vacuum

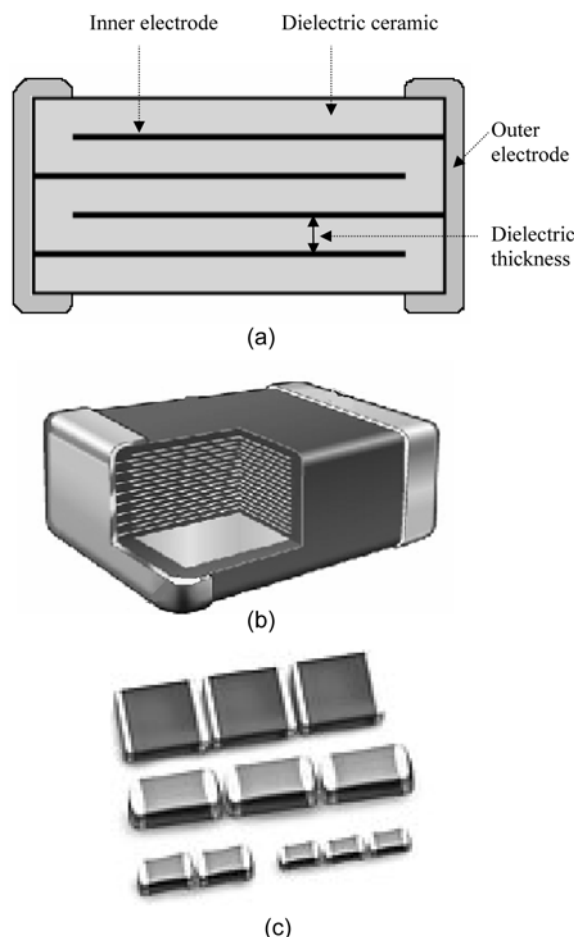


Fig. 1. (a), (b) A schematic and (c) picture of multilayer ceramic chip capacitors (MLCCs).

($=8.85 \text{ pF/m}$), ϵ_r is the relative dielectric constant of the material, N is the number of layers, A is the electrode area, and d is the dielectric thickness. In order to enhance the capacitance per unit volume, therefore, current efforts

*Corresponding author:
 Tel : +82-53-810-2561
 Fax: +82-53-810-4628
 E-mail: dhyoon@ynu.ac.kr

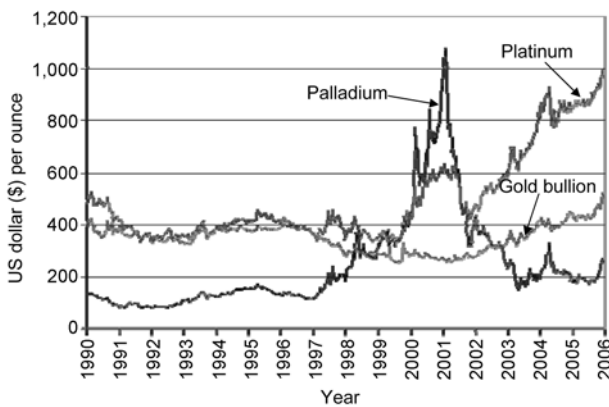


Fig. 2. Palladium prices compared to other precious metals from 1990 until 2006 [6].

are focusing on increasing the dielectric constant of the material as well as on decreasing the layer thickness. Among many candidate materials, BaTiO_3 with a dielectric constant of several thousand, which is much higher than that of most other ceramics, has maximized the volumetric efficiency [8]. Therefore, most of MLCCs currently being produced with a structure based on this powder have additions of small amounts of other additives to modify their electric, mechanical and thermal characteristics. Table 1 shows the several MLCC characteristics including approximate dielectric constant, temperature coefficient of capacitance, and relative BaTiO_3 content for the corresponding application based on the Electrical Industry Alliance (EIA) specifications [9]. An MLCC having the highest volumetric efficiency is currently as thin as $1 \mu\text{m}$ and is comprised of several hundred dielectric layers, and this thickness is expected to become thinner in the future in order to replace Ta- and Al-electrolytic capacitors [10-12]. The most widely used size of MLCC based on the EIA specification is 0603 ($1.6 \text{ mm} \times 0.8 \text{ mm}$) for general electronic equipment, 0402 ($1.0 \text{ mm} \times 0.5 \text{ mm}$) for mobile equipment, and 0201 ($0.4 \text{ mm} \times 0.2 \text{ mm}$) size MLCCs are being put into practical application [12]. Because the general belief is that each sintered layer of an MLCC needs at least 5 grains to ensure reliability [3, 13], BaTiO_3 powder being much finer than the thickness of the dielectric layer with stringent characteristics is essential for an industrial application. However, it is known that the tetragonality ($=c/a$), which is the source of the high dielectric constant, diminishes with a decrease in BaTiO_3 particle size and disappears below a critical particle

size [3].

Acquiring high quality BaTiO_3 particles is a prerequisite for the production of a reliable MLCC even though the MLCC production process is complicated, requiring many different fields of knowledge including powder processing, slip behavior, tape casting and sintering behavior in a reducing atmosphere, etc. Therefore, this author will start by introducing recent experimental results on nano- BaTiO_3 synthetic methods and their characteristics for MLCC applications in this review. The critical particle size of the cubic-to-tetragonal transformation and the resultant tetragonality values of synthesized powders including an explanation of our recent results will follow.

Hydrothermal vs. Solid-state Reaction Method

Easy powder dispersion with a spherical shape, low firing temperature with a high sintering density, high dielectric constant with a low dissipation factor, and consistent properties along with little lot-to-lot variation are the most desired properties of BaTiO_3 particles in the MLCC industry [3]. Many synthetic methods have been utilized to produce fine BaTiO_3 particles including using a solid-state reaction [14], co-precipitation (e.g., citrates [15], oxalates [16]), hydrothermal synthesis [17], a solvothermal method [18], alkoxide hydrolysis [19], a catecholate process [20], and metal-organic processing [21]. The powders produced by the hydrothermal method and the solid-state reaction are the most commonly used in the MLCC industry nowadays, after considering the powder properties and the cost of each method.

The hydrothermal method, which belongs to the category of liquid phase reactions, characteristically produces extremely fine particles with a narrow size distribution maintaining a spherical morphology [22]. This technique utilizes heating an aqueous suspension of insoluble salts in an autoclave at a moderate temperature and pressure so that the crystallization of a desired phase will take place. The advantages of hydrothermal crystallization are the reduced energy costs due to the modest temperatures sufficient for the reaction, less pollution, simplicity in the process equipment, and the enhanced rate of the precipitation reaction [22]. The particle size of hydrothermally-synthesized BaTiO_3 is usually less than 200 nm which is adequate for the thin layer application. Despite the above advantages, there

Table 1. Classification of MLCCs based on the Electrical Industry Alliance (EIA) specification [9]

Designation	Class	Temperature range ($^{\circ}\text{C}$)	Dielectric constant	Temperature coefficient (%)	BaTiO_3 content (wt.%)
NPO	1	-55~125	~ 100	± 30 (ppm)	10~50
X5R	2	-55~85	~ 4,000	± 15	90~98
X7R	2	-55~125	~ 4,000	± 15	90~98
Z5U	2	-10~85	~ 14,000	+22, -56	80~90
Y5V	2	-30~85	~ 18,000	+22, -82	80~90

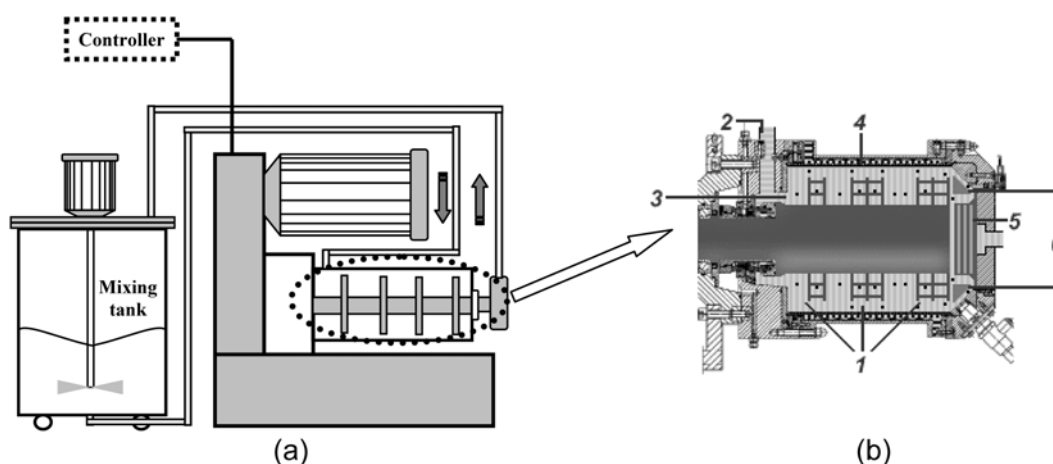


Fig. 3. Schematic of the (a) operating system and (b) the grinding chamber of a high energy mill [35]. 1: Rotor with discs, 2: inlet, 3: grinding media, 4: cooling jacket, 5 and 6: separation system.

is a shortcoming associated with this method. Due to the process condition of a high water pressure, large amounts of protons and hydroxyl ions tend to be incorporated into the BaTiO_3 lattice during the hydrothermal process [23]. As a result, a considerable enlargement of the unit cell volume, which gives a particle density lower than the ideal density, and a suppression of the tetragonal distortion of the perovskite unit cell are observed [24]. Moreover, it is reported that the MLCC made from hydrothermal powder shows a 'bloating' in the final stage of sintering due to the evolution of these incorporated defects, which is not observed in the powder derived from a solid-state reaction [23].

The solid-state reaction method is the most traditional one for preparing BaTiO_3 powders by mixing the starting materials, usually titanium oxide and barium carbonate, and calcining them at an elevated temperature around 1100-1400 °C [25, 26]. The powder from this method had been known to result in a significant amount of agglomeration, poor chemical homogeneity along with a coarse particle size due to the treatment at high temperature. However, a few researchers [27-31] have lately synthesized BaTiO_3 powders of 200 nm approximate size by a solid-state reaction below 1000 °C with the help of recently-available advanced milling facilities and very fine starting materials. A mechanochemical activation by the heavy milling is the key step in this recent process which alters the physicochemical properties of the starting materials and the mechanism of synthesis. Moreover, it is expected that the fine starting materials enhance the solid-state reaction due to their high activity, and hence decrease the reaction temperature and the final particle size [27-33]. Conventional ball mills and attrition mills adopting a discontinuous operating system have been used for a long time for the purpose of milling. On the other hand, modern high energy mills use a continuous operating system equipped with a high speed rotor rotating up to

several thousands times per minute, disc agitators and a cooling system. Their high energy input and the use of small grinding media with a diameter of 0.02-0.5 mm allow the achievement of a very small particle size down to the nanometer range in a very short processing time [34]. A schematic of a high energy mill is shown in Fig. 3 [35].

The typical weight losses of the solid-state reacted and the hydrothermally produced BaTiO_3 powders are compared in Fig. 4 [36]. The thermo-gravimetric analysis (TGA) result of hydrothermal powder in air shows a 1.2% of weight loss up to 1000 °C, which is much greater than that of a solid-state reacted powder which is less than 0.3 wt.%. This additional weight loss of hydrothermal powder is attributed to the release of defects such as hydroxyl ions (OH^-), protons (H^+) and carbonate ions (CO_3^{2-}), which are incorporated into the lattice during the synthesis at a high water pressure as explained above [23].

We have also recently synthesized 210 nm Ca-doped BaTiO_3 powder by a solid-state reaction by applying

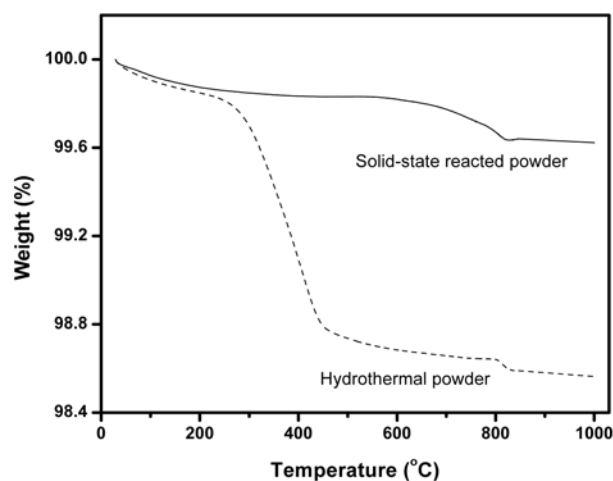


Fig. 4. Comparison of thermo-gravimetric behavior between solid-state reacted and hydrothermal BaTiO_3 powders [36].

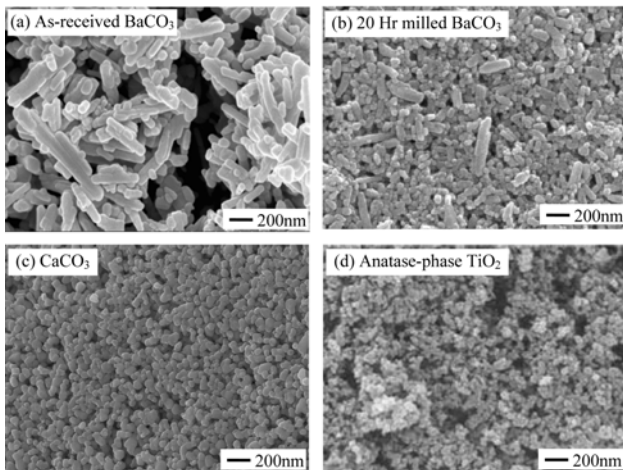


Fig. 5. SEM micrographs of the starting materials used in the synthesis of Ca-doped BaTiO₃ powder: (a) as-received BaCO₃, (b) 20 hour high-energy milled BaCO₃, (c) CaCO₃ and (d) anatase-phase TiO₂ [37].

the mechano-chemical activation of the starting materials [37]. According to Sakabe *et al.* [10], calcium ions occupying Ti-sites result in an increase of insulation resistance and the reliability of MLCCs by decreasing the mobility of oxygen vacancies compared to that with Ca-free BaTiO₃, which is the reason for Ca-doping in our experiment. In the synthesis of fine (Ba_{0.98}Ca_{0.02})_{1.002}TiO₃ powder, nano-sized BaCO₃, CaCO₃ and anatase-phased TiO₂ particles are used as starting materials. Since most of the nano-sized BaCO₃ particles have a needle-like shape, this powder is exposed to heavy high energy milling at first to decrease its size. SEM images of the starting materials including high energy milled BaCO₃ particles are shown in Fig. 5. The purpose of this mechano-chemical activation by high energy milling is to increase the contact points and the activity of the starting materials, and hence to get the fine Ca-doped BaTiO₃ powders at a low reaction temperature. It has been reported that the fine particles of TiO₂ act as a catalyst for the decomposition of BaCO₃ [28], and the anatase-phased TiO₂ has a higher activity and is more efficient in lowering the reaction temperature than the rutile one due to its low density (Density of anatase phase TiO₂=3.90 g/cm³, while that of the rutile phase=4.23 g/cm³) [38]. According to the thermo-gravimetric/differential thermal analysis (TG/DTA) results, both of the mechano-chemical activation and the use of anatase-phase TiO₂ is effective in decreasing the reaction temperature, more exactly the BaCO₃ decomposition temperature, by almost 200 °C compared to the composition without milling and the use of the rutile phase TiO₂ as shown in Fig. 6 [37]. As a result 210 nm-sized Ca-doped BaTiO₃ particles can be synthesized, which show superior characteristics in terms of the dielectric constant and the temperature coefficient of capacitance when this powder is applied in a high capacitance X5R MLCC with a 1 μm layer thickness [37]. Figure 7

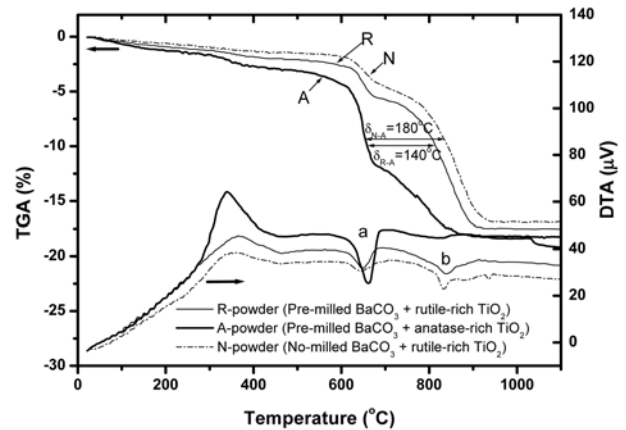


Fig. 6. Comparison of the solid-state reaction temperature using TG/DTA results among different combinations of starting materials in air with 3 K/minute of heating rate [37].

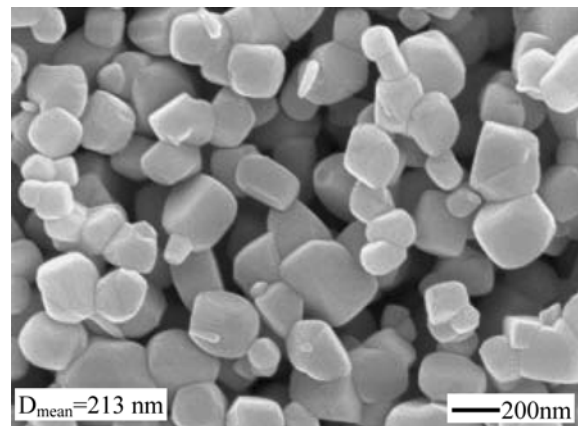


Fig. 7. SEM morphology of the synthesized Ca-doped BaTiO₃ powder after heat treatment at 985 °C for 2 hours. The average particle size is shown.

shows the SEM morphology of Ca-doped BaTiO₃ powder synthesized by heat treatment at 985 °C for 2 hour in an air atmosphere.

As explained above, the synthesis of nano-sized BaTiO₃ particles is possible nowadays by a solid-state reaction with the help of very fine starting materials and mechano-chemical activation using a high energy mill. In order to understand why nano-sized particles can be manufactured by a solid-state method, it is best to look into the reaction mechanism suggested by Beauger *et al.* [26] According to this model [26], BaTiO₃ is easily formed at the surface of TiO₂ particles which also act as the catalysts for BaCO₃ decomposition [28]. When the surface BaTiO₃ layer is formed by the decomposition of BaCO₃ and its reaction with TiO₂, the kinetics are governed by the barium and oxygen ion diffusion through this layer into the virgin TiO₂ phase. Since the TiO₂ phase never decomposes during the reaction, starting with fine TiO₂ particles is very beneficial in acquiring the final fine BaTiO₃ powder. Due to the excess of barium and oxygen ions in the surface layer, a Ba₂TiO₄ phase is generally formed initially [27-29,

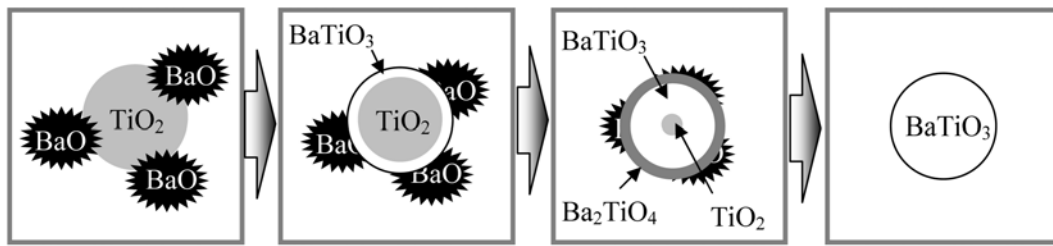
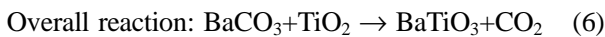


Fig. 8. Suggested solid-state reaction diagram for the formation of BaTiO₃ from BaCO₃ and TiO₂ [37].

31]. Homogeneous BaTiO₃ particles are formed gradually by the reaction between Ba₂TiO₄ and TiO₂ due to the continuous diffusion. This multi-step reaction mechanism is schematized in Fig. 8 [37]. The reaction equation is also represented in the following:



By considering the above reaction mechanism, one can estimate that a fine TiO₂ with a loose structure, *i.e.* low density like anatase-phase, enhances BaTiO₃ formation by decreasing both the length and activation energy for diffusion, which is consistent with our findings. Moreover, the use of very fine BaCO₃ particles is helpful in increasing the number of contact points with other starting materials and in their easy decomposition at low temperature.

Critical Particle Size on the Phase Transition

BaTiO₃ particles larger than 0.5 μm usually show a tetragonal-to-cubic phase transition at a Curie temperature which is generally located at 120-130 °C [39], although the Curie point is known to decrease accompanied by a decrease in the particle size of BaTiO₃. Uchino *et al.* [40] showed that the transition from tetragonal-to-cubic symmetry occurred at a critical particle size of 0.12 μm at 75 °C. The cubic phase shows paraelectric properties with a trivial dielectric constant, while the tetragonal phase shows ferroelectric properties which are more interesting for dielectric applications due to its high dielectric constant. In the temperature range for the cubic phase, *i.e.* above the Curie point, the ideal perovskite structure of a cubic and symmetrical unit cell is stable. Between 0 °C and the Curie point, BaTiO₃ shows a distorted perovskite structure in which the Ti⁴⁺ and O²⁻ ions are displaced in the opposite direction from their original positions, whereas the barium ion does not change its position [41]. A perovskite crystal structure, the displacement of the Ti⁴⁺ and O²⁻ ions and the slight distortion of oxygen octahedra during the cubic to tetragonal phase

transition are shown in Fig. 9 [42].

Needless to say, industry needs very fine BaTiO₃ powders with high dielectric constants to manufacture high capacitance MLCCs. By contrast, it is known that the dielectric constant decreases with a decrease in particle size and disappears below a certain critical size. This is due to the phase transition from tetragonal-to-cubic in connection with the particle size decrease, which is called the size effect [22, 40, 43-45]. According to Jaffe *et al.* [46], physical parameters such as chemical purity, surface defects, particle size [40, 47] and the sintering conditions affect this critical particle size [46].

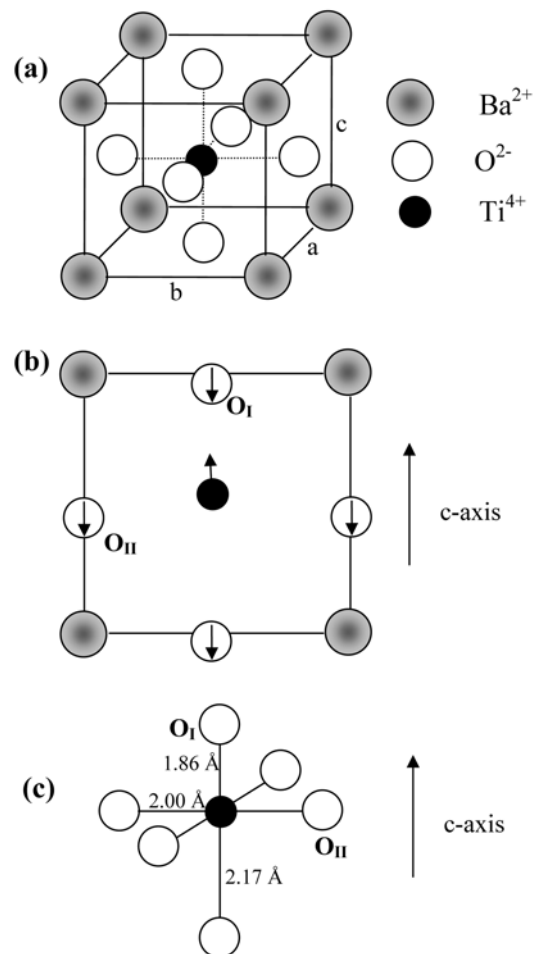


Fig. 9. (a) Perovskite structure of BaTiO₃ above the Curie point, (b) a-axis projection of tetragonal BaTiO₃ with atomic displacements, and (c) [TiO₆] octahedron in the tetragonal phase showing the displacement of Ti along the c-axis [42].

Begg *et al.* [45], in addition, reported that hydrothermal BaTiO₃ powder with a particle size larger than 0.27 μm was completely tetragonal and with a particle size less than 0.19 μm was a fully-cubic phase. More detailed reports on the critical particle size of the BaTiO₃ phase transition are presented in Table 2. All the reports show differences in the critical particle size. This difference in critical size may come from the different powder characteristics related with the synthetic method as well as the resolution of equipment used for the characterization. For example, X-ray diffraction usually does not detect a small portion with a tetragonal content, while Raman spectroscopy may do [43, 44].

In order to explain this room temperature stabilization of the cubic structure in a fine-grained BaTiO₃, two models have been proposed: one is the phenomenological surface layer model [48], and the other is the pure phase model [22, 40]. The phenomenological surface layer model is based on the structural transition between the outer cubic surface layer of fixed thickness and the tetragonal core, with a gradient of tetragonality existing between the two regions. As the particle size decreases, the relative ratio of the cubic-to-tetragonal region is increased and eventually only a stable cubic region

remains at a critical particle size.

The pure phase model does not require the coexistence of the cubic and tetragonal structures. There are two mechanisms to explain this model; strains imposed by the presence of lattice hydroxyl ions [22] and the role of a surface [40]. Regarding the hydroxyl ion effects, Vivekanandan and Kutty [22] explained the source of lattice strain as from point defects caused by the presence of hydroxyl ions and the corresponding cation vacancies. According to them, the residual hydroxyl ions in the oxygen sub-lattice retained during the hydrothermal BaTiO₃ synthetic process are compensated by cation vacancies, and result in strain leading to the metastable presence of the cubic phase at room temperature. The surface effect model is based on the surface tension associated with the very fine powder stabilizing the cubic phase at room temperature. Uchino *et al.* [40] observed a decrease in room temperature tetragonality and in the Curie point as a function of a particle size reduction. According to them [40], this surface tension is sufficiently high to decrease the tetragonality and the Curie point in the small particle sized BaTiO₃.

Looking to our recent research results on the tetragonality (the relative ratio of the lattice parameter of

Table 2. Research results on the critical particle size of the cubic-to-tetragonal phase transition for BaTiO₃

Researcher	Results	Preparation method	Measurement method
Arlt <i>et al.</i> [44]	≤500 nm pseudocubic	oxalate	XRD, ϵ_r
Uchino <i>et al.</i> [40]	≤120 nm cubic >120 nm tetragonal	hydrothermal, solid-state, coprecipitation	XRD, BET
Hennings & Schreinemacher [24]	≤400 nm cubic ≥200 nm tetragonal	hydrothermal solid-state solid-state	XRD
Begg <i>et al.</i> [45]	≤190 nm cubic ≥270 nm tetragonal	hydrothermal	XRD, SEM, HRTEM
Takeuchi <i>et al.</i> [50]	320-1220 nm coexistence	solid-state	XRD
Lobo <i>et al.</i> [51]	≥200 nm tetragonal	sol-gel	XRD, ϵ_r
Frey & Payne [52]	≥100 nm tetragonal	alkoxide	XRD, Raman
Wada <i>et al.</i> [53]	≤200 nm cubic	hydrolysis	XRD
Li & Shih [54]	≤56 nm cubic ≥71 nm tetragonal	alkoxide-hydroxide	XRD
Sakabe <i>et al.</i> [43]	≤70 nm cubic	hydrolysis	Raman, XRD
Jiang <i>et al.</i> [55]	105-130 nm	sol-gel Cubic to tetragonal change	Raman XRD
Lu <i>et al.</i> [56]	≤3500 nm cubic 80 nm Mainly cubic	stearic-acid gel hydrothermal	XRD, DSC Raman
Kong <i>et al.</i> [27]	≥3,000 nm tetragonal	solid-state	XRD
Sakabe <i>et al.</i> [10]	≥200 nm tetragonal	hydrolysis	XRD
Maison <i>et al.</i> [20]	≥230 nm tetragonal	catecholate process	XRD
Xu & Gao [57]	70 nm 80% tetragonal	hydrothermal	XRD, DSC
Kim <i>et al.</i> [58]	100 nm 82% cubic	hydrothermal	NMR, Raman
Lee <i>et al.</i> [59]	150 nm tetragonal	spray pyrolysis	XRD
Qi <i>et al.</i> [60]	240 nm tetragonal	hydrothermal	XRD, DSC
Kwon <i>et al.</i> [61]	≥100 nm tetragonal	solvothermal	XRD
Kwon & Yoon [49]	≤170 nm cubic	hydrothermal	XRD
Ryu & Yoon [62]	≥54 nm tetragonal	solid-state	XRD

the *c*- to the *a*-axis, $=c/a$) of hydrothermal BaTiO₃ powder with particle growth inhibitors added [49], it seems that the mechanism of cubic stabilization in fine BaTiO₃ particles is not affected by the incorporated defects but mainly by the large surface tension. In this experiment, we tried to enhance the dielectric constant of fine hydrothermal BaTiO₃ powders by eliminating the internal defects using heat treatment at various temperatures. The behavior of the tetragonality ($=c/a$), an indirect measure of dielectric constant, was investigated as a function of the particle size and the processing temperature. Different amounts of growth inhibitors such as carbon black and corn starch were added to minimize the drawbacks of heat treatment such as hard agglomeration and particle growth. Based on the experimental results [49], controlling the particle size under the same heat treatment condition is possible by using growth inhibitors, where carbon black is a more efficient inhibitor than corn starch due to its high burnout temperature compared to that of corn starch as shown in Fig. 10. Most of the corn starch is burnt up to

300 °C, while carbon black exists up to almost 600 °C acting as a more efficient particle growth inhibitor. The tetragonality ($=c/a$) increases gradually between a particle size of 170-330 nm and shows saturation for a particle size larger than 330 nm as shown in Fig. 11. However, it is found that the tetragonality enhancement by heat treatment above 950 °C while minimizing the particle growth is not efficient as shown in Fig. 12. These results indicate the relatively smaller contribution from the internal defects than the free surface in stabilizing the metastable cubic phase and/or a high enough thermal energy corresponding to heat treatment at 950 °C or a higher temperature for the removal of internal defects.

In summary, due to the importance of fine tetragonal BaTiO₃ powder with a high dielectric constant, many researchers have been interested in the cubic-to-tetragonal phase transition of this powder. However, all the research reports show different results on a critical particle size. This discrepancy may come from the different residual elastic strain energy, chemical impurity levels and crystalline defects associated with various powder synthetic methods as well as the resolution of the characterization.

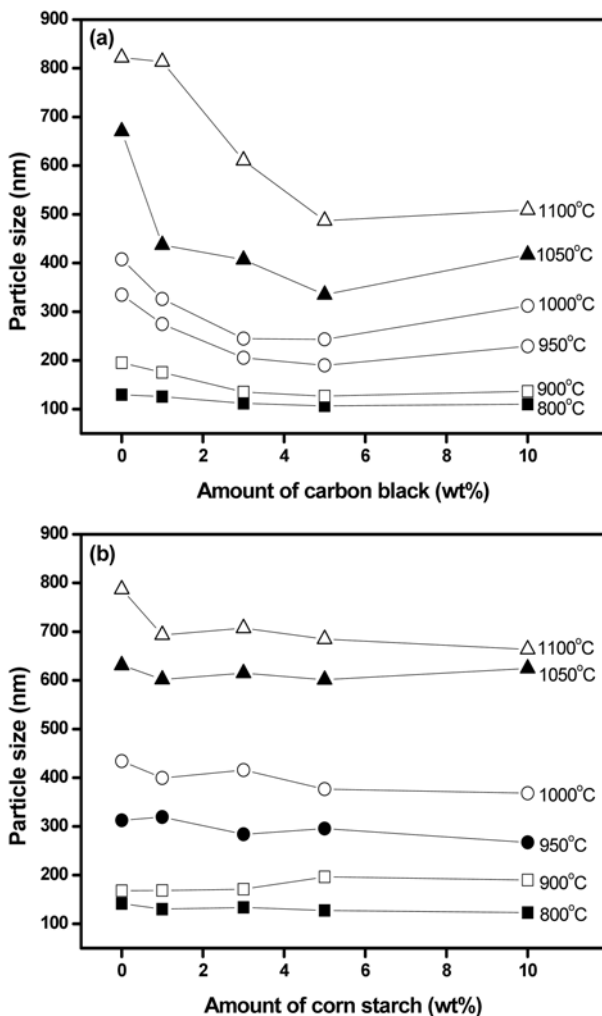


Fig. 10. Comparison of particle size of hydrothermal BaTiO₃ powder heat treated at various temperatures with different amounts of (a) carbon black and (b) corn starch [49].

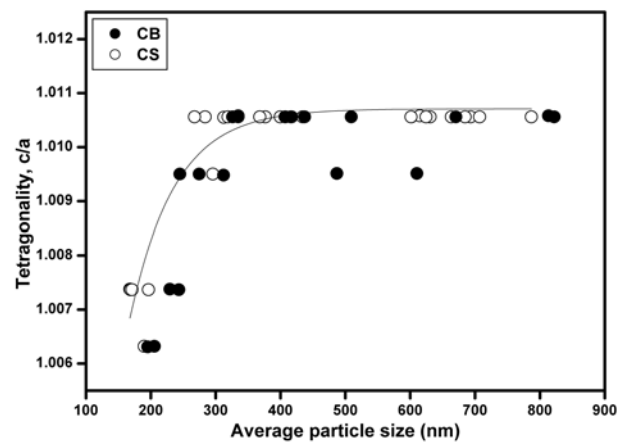


Fig. 11. The relationship between tetragonality ($=c/a$) and the average particle size of hydrothermal BaTiO₃ powder heat treated with various amounts of carbon black and corn starch [49].

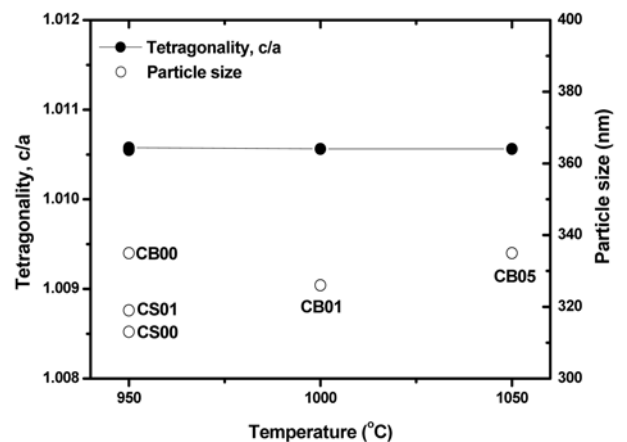


Fig. 12. The relationship between tetragonality and processing temperature of hydrothermal BaTiO₃ powder having similar particle sizes [49].

Tetragonality of Fine BaTiO₃ Particles

Most industries prefer to use spherical, chemically homogeneous and unagglomerated fine BaTiO₃ powders with a high dielectric constant. Even though Wada *et al.* suggested a direct dielectric constant measurement method using a particle [53], which is called a modified powder dielectric measurement method, researchers prefer to use an indirect method to estimate the dielectric constant of BaTiO₃ powder because there is some controversy on the newly suggested above method yet. The most widely used indirect method is the calculation of the tetragonality ($=c/a$) based on the XRD data. It can be easily shown that the high dielectric constant of BaTiO₃ powder is correlated with its high tetragonality which originates from the tetragonal distortion of the lattice [41].

Figure 13 shows XRD patterns of a cubic BaTiO₃ powder without the {200} peak splitting, and a tetragonal one with a peak splitting of the (200) and (002) planes for $2\theta=44-46^\circ$. The tetragonality is measured from the lattice parameters of the c- and a-axes which can be calculated using Bragg's law. The MLCC industry prefers BaTiO₃ powders with a tetragonality higher than 1.008, along with an average particle size of approximately 200 nanometers, especially for the high capacitance X5R or X7R applications [63].

Our recent experimental results on the relationship between tetragonality and the average particle size using a hydrothermal powder are demonstrated further in Fig. 11 [49]. The maximum tetragonality obtainable by heat treatment is 1.0105 with the particles larger than 330 nm, and a tetragonality greater than 1.008 is obtained with BaTiO₃ particles larger than 230 nm. It is found that the tetragonality is a function of the particle size. The tetragonality of a hydrothermal BaTiO₃ having a particle size smaller than 300 nm decreases drastically to 200 nm and can not be measured for particles smaller than 170 nm because the local (002) peak cannot

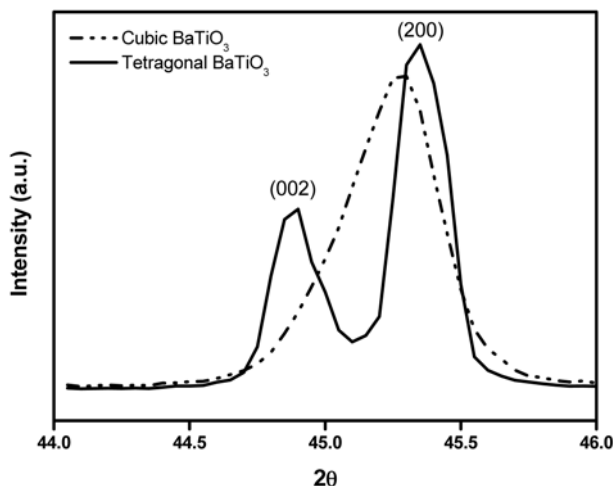


Fig. 13. XRD patterns from a cubic BaTiO₃ showing one peak and a tetragonal BaTiO₃ with peak splitting at $2\theta=44-46^\circ$ [63].

be distinguished. According to Uchino *et al.* [40], the maximum tetragonality is 1.0095 for a single crystal which is smaller than our observation. On the other hand, the same maximum tetragonality of 1.0105 with a hydrothermal powder calcined at 1150 °C is also reported by Chen and Chen [64]. It is not difficult to estimate that a higher tetragonality of a powder than for a single crystal is possible if we consider the size effect on the cell polarizability. According to Kinoshita and Yamaji [65], when the particle size of BaTiO₃ decreases from 53 to 1.1 μm, the cell polarizability increases due to the reduced internal strain. This strain originates from the lattice parameter change associated with the cubic-to-tetragonal transition at the Curie temperature. It is easier to release this strain for small particles than for large ones. This means that a large single crystal contains more strain and resultantly shows a lower tetragonality than a small particle with less internal strain [66]. By decreasing the particle size further, however, the polarizability decreases because of the increased strains due to the high surface area as explained above [67]. In order to examine the relationship between tetragonality and processing temperature, 5 samples having similar particle sizes of approximately 330 nm among 60 samples were chosen. Their particle sizes and the corresponding tetragonality values are shown in Fig. 12. From this figure, it is noted that all the five samples with a similar particle size show the same tetragonality regardless of their processing temperature. This means that the tetragonality enhancement by heat treatment, while maintaining the particle size as small as possible by adding inhibitors, is not efficient, although it is conceptually possible by offering enough thermal energy required for the defect removal. This can be translated into two aspects, which the contribution of internal defects is not too high compared to the effect of the free surface in stabilizing the metastable cubic phase, or that the thermal energy corresponding to a heat treatment higher than 950 °C is large enough to remove the internal defects for the tetragonality enhancement of hydrothermal BaTiO₃. It seemed therefore that, an investigation of the factors associated with various synthetic routes necessitates instead a modification of hydrothermally-synthesized particles in order to increase the tetragonality while maintaining the small particle size of BaTiO₃.

Based on the other set of our experiments which was performed in order to increase the tetragonality using a solid-state reaction method, we have found that the tetragonality for fine powder could be enhanced by adequate treatments such as high energy milling and a 2-step heat treatment [62]. According to these results [62], 128 and 212 nm-sized BaTiO₃ powders show tetragonality values of 1.0097 and 1.0105 respectively, which are higher than other reported values with similar particle sizes. Using the same Ca-doped BaTiO₃ powder processed using the high-energy mill as explained in section 2,

the starting powder mixtures are exposed to 1- or 2-step heat treatment whose profiles are shown in Fig. 14. Figure 15 shows the XRD peaks for (002) and (200) planes of synthesized BaTiO_3 powder heat-treated at 900, 950 and 1000 °C by the 2-step heat treatment compared with that of powder prepared by the conventional 1-step heating at 950 °C for comparison. BaTiO_3 powder by the conventional heat treatment shows less tetragonal phase than that of the 2-step treatment, which is judged by the degree of peak separation between (002) and (200) planes after heat treatment at 950 °C. The calculated tetragonality is 1.0051 for the former whereas 1.0097 for the latter, which means that the 2-step heat treatment is more effective than the conventional heat treatment to get particles with a high tetragonality. A holding temperature of 800 °C for the 2-step heat treatment is determined by considering the BaCO_3 decomposition and the nanocrystalline cubic BaTiO_3 formation based on the TG/

DTA and XRD results. By holding the temperature at 800 °C for 1 hour, time is offered for CO_2 elimination and for the formation of cubic BaTiO_3 which resulted in the acceleration of the forward reaction in Eq. (6) by Le Chatelier's principle and the enhancement of tetragonality simultaneously. Figure 16 shows the SEM morphologies of BaTiO_3 powders synthesized at various temperatures by the 2-step heat-treatment. Characterization shows average particle sizes of 54, 128 and 212 nm, and specific surface areas of 13.50, 6.32 and 4.23 m^2/g , and tetragonalitys of 1.0000, 1.0097 and 1.0105 for the powders heat-treated at 900, 950 and 1000 °C, respectively.

Table 3 summarizes the recent research results of synthesized BaTiO_3 characteristics including the particle

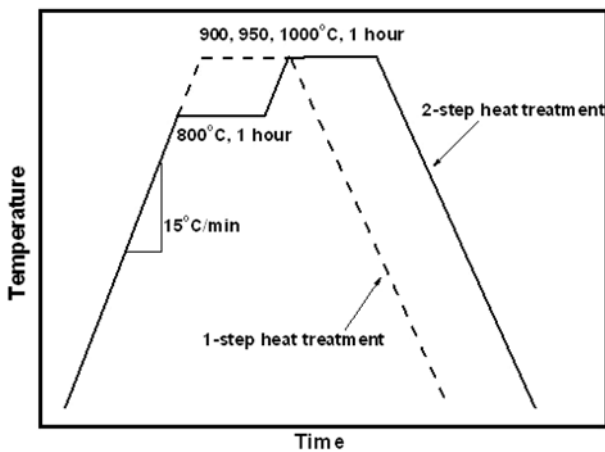


Fig. 14. Schematic of 2 step heat-treatment profile used to enhance the tetragonality of solid-state reacted BaTiO_3 powder [62].

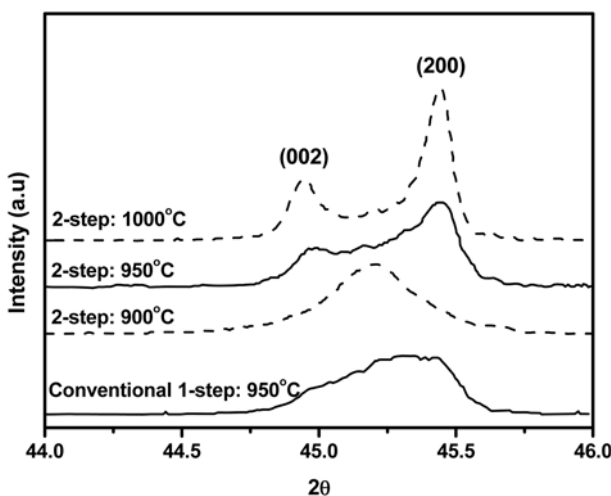


Fig. 15. The XRD patterns of BaTiO_3 powders synthesized at different temperatures using the 2-step heat treatment for $2\theta=44-46^\circ$. The peak from BaTiO_3 prepared by a conventional heat treatment at 950 °C is included for comparison [62].

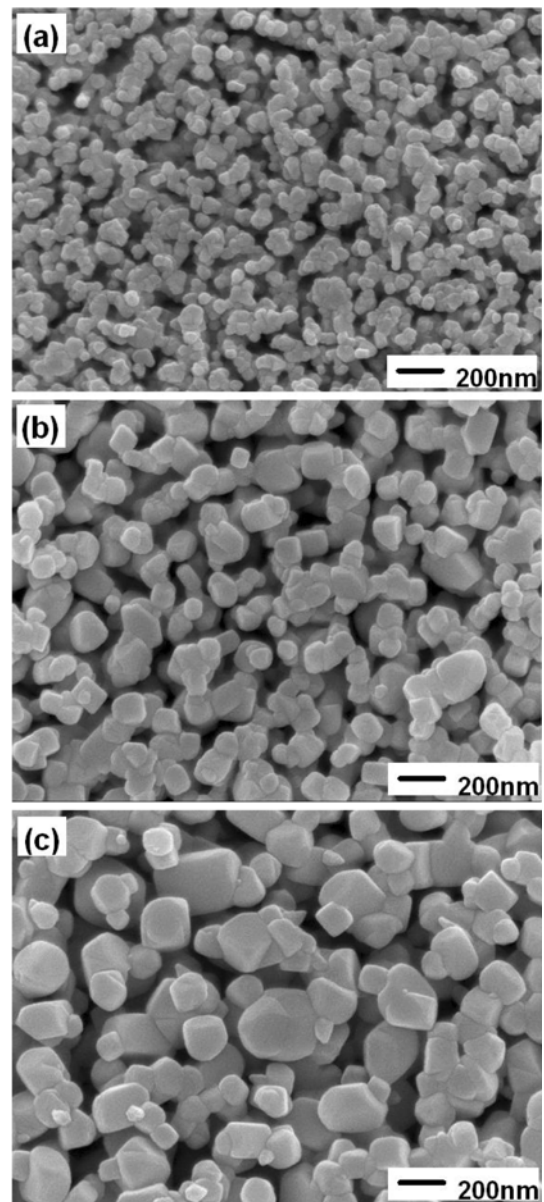


Fig. 16. SEM morphologies for BaTiO_3 powders synthesized at (a) 900, (b) 950 and (c) 1000 °C for 1h in air by the 2-step heat treatment [62].

Table 3. Recent research results on the tetragonality of synthesized BaTiO₃

Researcher	Processing temperature (°C)	Particle size (nm)	Tetragonality (=c/a)	Preparation method
Uchino <i>et al.</i> [40]	-	-	1.0095	single crystal
	-	120	cubic	hydrothermal
	-	200	1.006	coprecipitation
	-	300	1.009	solid-state reaction
Sakabe <i>et al.</i> [43]	1000	290	1.008	hydrolysis
Kong <i>et al.</i> [27]	1100	-	cubic	hydrothermal
	1150	3000	1.01	
Maison <i>et al.</i> [20]	950	230	1.0080	catecholate process
	1000	240	1.0086	
	1100	400	1.0098	
Chen & Chen [64]	900	-	cubic	hydrothermal
	1150	-	1.0105	
Ando <i>et al.</i> [33]	900	-	cubic	solid-state reaction
Kwon & Yoon [49]	800	<170	cubic	hydrothermal
	950	335	1.0105	
Sakabe <i>et al.</i> [10]	1050	200	1.0095	hydrolysis (Ca-doped BaTiO ₃)
Tsurumi <i>et al.</i> [68]	-	125	1.0067	solid-state reaction (Commercial powders)
	-	130	1.0081	
	-	158	1.0084	
	-	194	1.0097	
Ryu & Yoon [62]	900	54	cubic	solid-state reaction (Ca-doped BaTiO ₃)
	950	128	1.0097	
	1000	212	1.0105	

sizes and the corresponding tetragonality values. It is clear that our research utilizing 2-step heat treatments shows higher tetragonality values with finer BaTiO₃ particle sizes than any other reports. This is due to the use of very fine starting materials including fine-milled BaCO₃ and anatase-rich TiO₂, and the application of the 2-step heat-treatment process. Inevitable grain growth during the high temperature treatment of solid-state BaTiO₃ synthesis can be also minimized by decreasing the reaction temperature.

Outlook

Much effort has been concentrated to increase the volumetric efficiency of a MLCC by increasing the number of layers and by decreasing the dielectric thickness in the last decade, and the results are fruitful so far as shown in Fig. 17 [69]. There was skepticism during the late 1990s that the minimum dielectric thickness produced by tape casting could not be less than 3 μm [70], however, industry produces reliable MLCCs with thinner than 1 μm dielectric layers using the same tape casting method. This author strongly believes that three features have driven the current large progress. One is the continuous improvement in nano-sized BaTiO₃ particle synthesis and its powder characteristics. The second is an improvement in manufacturing equipment including tape casters, screen printers, stackers, etc. The third is a technical breakthrough in the dispersion of ceramic powder and slip which are related with the new introduction of high energy mills.

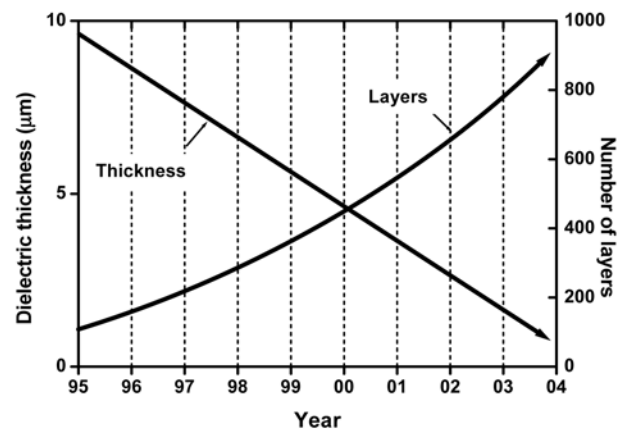


Fig. 17. Trends of the change in dielectric thickness and number of layers of MLCCs during the last 10 years [69].

However, the reduction in dielectric thickness using a tape caster seems to meet a limitation within several years due to the characteristics of this method. Since the slip is poured into a reservoir behind the doctor blade and the carrier film to be cast upon is set in motion to form a thin ceramic tape, it is not easy to get tapes thinner than 1 μm. This is why many researchers have been moving to produce MLCCs using film methods such as sputtering [71, 72], metal organic chemical vapor deposition [73, 74] and pulsed laser deposition [75-78]. MLCCs have covered a wide range of current capacitor applications as shown in Fig. 18 [69]. However, electrolytic capacitors using Ta and Al are still occupying the high capacitance region beyond 100 μF. In order to

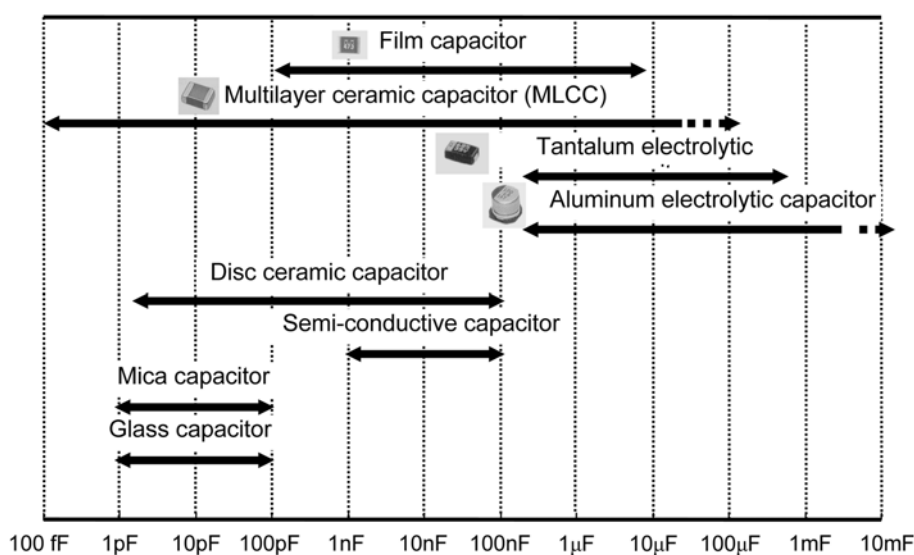


Fig. 18. Capacitance ranges for various capacitors [69].

replace these Ta- and Al-electrolytic capacitors by MLCCs, continuous technical innovations are required.

Passive electronic components including MLCCs are conventionally mounted onto a printed circuit board, which results in high parasitic capacitance and a low clock speed [1]. A recently emerging new technology, which is termed “embedded passive components” in a system on packaging, is to fabricate passive components such as capacitors, resistors and inductors into printed wiring boards during the fabrication process [79-81]. This embedded passive technology is believed to have merits such as better electrical performance and higher volumetric efficiency with less cost. The passive components may be placed directly below active devices using this technique. As a part of these efforts, fine BaTiO₃ particles are dispersed in a polymeric matrix such as an epoxy resin [82]. However, one of the serious obstacles here is the low capacitance that can be realized with this passive form. Therefore, this author believes that continuous efforts are expected for a while both in increasing the volumetric efficiency of a MLCC and in the utilization of new technology including an embedded passive system.

Acknowledgements

This work was supported by the Korea Research Foundation Grant funded by the Korean Government (MOEHRD) (KRF-2005-003-D00126). This author would like to thank Drs. K. H. Hur and S. K. Lee at Samsung Electro-Mechanics Co. and Dr. S. S. Ryu at KICET for their helpful advice and discussions.

References

1. B.I. Lee, P. Badheka, D.H. Yoon, V. Magadala, and M. Wang, *J. Ceram. Proc. Res.* 5[2] (2002) 127-132.
2. G.N. Howatt, R.G. Brekenridge, and J.M. Brownlow, *J. Am. Ceram. Soc.* 30[8] (1947) 237-242.
3. D.H. Yoon and B.I. Lee, *J. Ceram. Proc. Res.* 3[2] (2002) 41-47.
4. Y. Sakabe, in *Proceedings of the 9th US-Japan Seminar on Dielectric and Piezoelectric Ceramics*, November 1999, (Japan, 1999) p.1.
5. D.F.K. Hennings, *J. Eur. Ceram. Soc.* 21 (2001) 1637-1642.
6. Web-site of [UNCTAD based on data from Johnson Matthey's Platinum Report] <http://www.unctad.org/infocomm/anglais/palladium/prices.htm#pricelinks>, as on 25 July 2006.
7. J.M. Herbert, in “*Ceramic Dielectrics and Capacitors*” (Gordon and Breach Science Publishers, New York, 1985) p.9.
8. G. Goodman, R.C. Buchanan, and T.G. Reynolds III, in “*Ceramic Materials for Electronics*” edited by R. C. Buchanan, 2nd Ed. (Marcel Dekker, New York, 1991) p.69.
9. Electrical Industry Alliance (EIA), *World Capacitor Trade Statistics (WCTA)* (2004).
10. Y. Sakabe, N. Wada, T. Hiramatsu, and T. Tonogaki, *Jpn. J. Appl. Phys.* 41 (2002) 6922-6925.
11. S. Wada, H. Yasuno, T. Hoshina, S.M. Nam, H. Kakemoto, and T. Tsurumi, *Jpn. J. Appl. Phys.* 42 (2003) 6188-6195.
12. H. Kishi, Y. Mizuno, and H. Chazono, *Jpn. J. Appl. Phys.* 42 (2003) 1-15.
13. Y. Sakabe, in “*Ceramic Transactions*” edited by J.H. Jean, T.K. Gupta, K.M. Nair, and K. Niwa, Vol. 97 (American Ceramic society, OH, 2000) p.1.
14. L.K. Templeton and J.A. Pask, *J. Am. Ceram. Soc.* 42 (1959) 212-216.
15. B.J. Mulder, *J. Am. Ceram. Soc. Bull.* 49 (1970) 990-993.
16. M. Stockenhuber, H. Mayer, and J.A. Lercher, *J. Am. Ceram. Soc.* 76[5] (1993) 1185-1190.
17. H. Kumazawa, S. Annen, and E. Sada, *J. Mat. Sci.* 30 (1995) 4740-4744.
18. D. Chen and X. Jiao, *J. Am. Ceram. Soc.* 83[10] (2000) 2637-2639.
19. P.P. Phule, S. Raghavan, and S.H. Risbud, *J. Am. Ceram. Soc.* 70[5] (1987) C-108-C-109.
20. W. Maison, R. Kleeberg, R.B. Heimann, and S. Phanichphant, *J. Eur. Ceram. Soc.* 23 (2003) 127-132.

21. A.S. Shaikh and G.M. Vest, *J. Am. Ceram. Soc.* 69 (1986) 682-688.
22. R. Vivekanandan and T.R.N. Kutty, *Powder Technology* 57 (1989) 181-192.
23. D.F.K. Hennings, C. Metzmaier, and B.S. Schreinemacher, *J. Am. Ceram. Soc.* 84[1] (2001) 179-182.
24. D. Hennings and S. Schreinemacher, *J. Eur. Ceram. Soc.* 9 (1992) 41-46.
25. M. Vieth, S. Mathur, N. Lecercf, V. Huch, T. Decker, H. Beck, W. Wiser, and R. Haberkorn, *J. Sol-gel Sci. Technol.* 15 (2000) 145-158.
26. A. Beauger, J. Mutin, and J. Niepce, *J. Mater. Sci.* 18 (1983) 3041-3047.
27. L.B. Kong, J. Ma, H. Huang, R.F. Zhang, and W.X. Que, *J. Alloys & Comp.* 337 (2002) 226-230.
28. E. Brzozowski and M.S. Castro, *Thermochimica Acta* 398 (2003) 123-129.
29. C. Gomez-Yanez, C. Benitez, and H. Balmori-Ramirez, *Ceram. Int.* 26 (2000) 271-277.
30. M.T. Buscaglia, M. Bassoli, and V. Buscaglia, *J. Am. Ceram. Soc.* 88 (2005) 2374-2379.
31. V. Berbenni, A. Marini, and G. Bruni, *Thermochimica Acta* 374 (2001) 151-158.
32. E. Brzozowski and M.S. Castro, *J. Eur. Ceram. Soc.* 20 (2000) 2347-2351.
33. C. Ando, R. Yanagawa, H. Chazono, H. Kishi, and M. Senna, *J. Mater. Res.* 19[12] (2004) 3592-3599.
34. C. Warnke, in "Operational Modes of Agitator Bead Mills" (NETZSCH-Feinmahltechnik GmbH, Germany, 2003) p.9.
35. Web-site of "Chicago Boiler Company," <http://www.cbmills.com>, as on 1 June 2006.
36. D.H. Yoon, in Barium Titanate Tape Properties for MLCC Application Using Different Binder Systems, Ph. D. Dissertation (Clemson University, SC, 2003) p.116.
37. S.S. Ryu, S.K. Lee, and D.H. Yoon, Submitted to *J. Electro. Ceram.* (2006).
38. M.J. O'neil, A. Smith, P.E. Heckelman, J.R. Obenchain, J.A.R. Gallipeau, M.A. D'Arecca, and S. Budavari, in *The Merck Index* (MERCK & CO., 2001) p.9549.
39. W. Kanzig, *Ferroelectricity*. 74 (1987) 285-291.
40. K. Uchino, E. Sadanaga, and T. Hirose, *J. Am. Ceram. Soc.* 72[8] (1989) 1555-1558.
41. W. Cochran, *Adv. Phys.* 9 (1960) 387-406.
42. V. Anuradha, in *NMR Study of Quardrupolar Nuclei in Some Simple Cubic and Perovskite Compounds*, Masters Thesis (University of Warwick. U.K., 1990).
43. Y. Sakabe, N. Wada, and Y. Hamaji, *J. Kor. Phys. Soc.* 32 (1998) S260-S264.
44. G. Arlt, D. Hennings, and G.D. With, *J. Appl. Phys.* 58 (1985) 1619-1625.
45. B.D. Begg, E.R. Vance, and J. Nowotny, *J. Am. Ceram. Soc.* 77 (1994) 3186-3192.
46. B. Jaffe, W.R. Cooke, and H. Jaffe, in "Piezoelectric Ceramics" (Academic press, 1971) p.53.
47. K. Kinoshita and A. Yamaji, *J. Appl. Phys.* 47[1] (1976) 371-373.
48. J.C. Niepce, in "Surfaces and Interfaces of Ceramic Materials" (Kluwer Academic Publishers, Dordrecht, Netherlands, 1989) p.512.
49. S.W. Kwon and D.H. Yoon, *J. Eur. Ceram. Soc.* In Press (2006).
50. T. Takeuchi, K. Ado, T. Asai, H. Kageyama, Y. Saito, C. Masquelier, and O. Nakamura, *J. Am. Ceram. Soc.* 77[6] (1994) 1665-1668.
51. R. Lobo, D. Mohallem, and R. Moreira, *J. Am. Ceram. Soc.* 78[5] (1995) 1343-1346.
52. M.H. Frey and D.A. Payne, *Phys. Rev. B* 54[5] (1996) 3158-3168.
53. S. Wada, H. Yasuno, T. Hoshina, S.M. Nam, H. Kakemoto, and T. Tsurumi, *Jpn. J. Appl. Phys.* 42 (2003) 6188-6195.
54. X. Li and W. Shih, *J. Am. Ceram. Soc.* 80[11] (1997) 2844-2952.
55. B. Jiang, J.L. Peng, L.A. Bursill, T.L. Ren, P.L. Zhang, and W.L. Zhong, *Physica B*. 291 (2000) 203-212.
56. S.W. Lu, B.I. Lee, Z.L. Wang, and W.D. Samuels, *J. Cryst. Growth*. 219 (2000) 269-276.
57. H. Xu and L. Gao, *Jam. Ceram. Soc.* 86[1] (2003) 203-205.
58. Y.I. Kim, J.K. Jung, and K.S. Ryu, *Mater. Res. Bull.* 39 (2004) 1045-1053.
59. K.K. Lee, Y.C. Kang, K.Y. Jung, and J.H. Kim, *J. Alloys & Comp.* 395 (2005) 280-285.
60. L. Qi, B.I. Lee, P. Badheka, L.Q. Wang, P. Gilmour, W.D. Samuels, and G.J. Exarhos, *Mat. Lett.* 59 (2005) 2794-2798.
61. S.G. Kwon, K. Choi, and B.I. Kim, *Mat. Lett.* 60 (2006) 979-982.
62. S.S. Ryu and D.H. Yoon, *J. Mater. Sci.* In Press (2006).
63. S.W. Kwon and D.H. Yoon, *Ceram. Int.* In Press (2006).
64. K.Y. Chen and Y.W. Chen, *Powder Tech.* 141 (2004) 69-74.
65. K. Kinoshita and A. Yamaji, *J. Appl. Phys.* 47[1] (1976) 371-373.
66. G. Arlt, *Ferroelectrics* 104 (1990) 217-227.
67. A. Herczog, *IEEE Trans., PHP-9*[4] (1973) 247-256.
68. T. Tsurumi, T. Sekine, H. Kakemoto, T. Hoshina, S.M. Nam, H. Yasuno, and S. Wada, *J. Am. Ceram. Soc.* 89[4] (2006) 1337-1341.
69. Murata Report on Ceramic Capacitors, Murata Mfg. (2006).
70. L. Mann, Kemet Electronics Corp., Seminar given at Clemson Univ. (Clemson, SC, 2002).
71. S.S. Thony, H.W. Lehmann, and P. Gunter, *Appl. Phys. Lett.* 61 (1992) 373-375.
72. C.H.J. Huang and T.A. Rabson, *Opt. Lett.* 18 (1993) 811-813.
73. H.A. Lu, L.A. Wills, B.W. Wessels, W.P. Lin, T.G. Zhang, G.K. Wong, D.A. Neumayer, and T.J. Marks, *Appl. Phys. Lett.* 62 (1993) 1314-1316.
74. D.M. Gill, B.A. Block, C.W. Conrad, B.W. Wessels, and S.T. Ho, *Appl. Phys. Lett.* 69 (1996) 2968-2970.
75. N. Shu, A. Kumar, M.R. Alam, H.L. Chan, and Q. You, *Appl. Surf. Sci.* 109/110 (1997) 366-370.
76. K. Kaemmer, H. Huelz, B. Holzapfel, W. Haessler, and L. Schultz, *J. Phys. D: Appl. Phys.* 30 (1997) 522-526.
77. L. Beckers, J. Schubert, W. Zander, J. Ziesmann, A. Eckau, and P. Lienenbach, *J. Appl. Phys.* 83 (1998) 3305-3310.
78. S. Mustofa, T. Araki, T. Furusawa, M. Nishida, and T. Hino, *Mater. Sci. & Eng. B*103 (2003) 128-134.
79. R. Snogren, *Printed Circuit Fab.* 25[11] (2002) 26-29.
80. V.G. Shah and D.J. Hayes, *Printed Circuit Fab.* 25[9] (2002) 32-34.
81. J. Murray, *Printed Circuit Fab.* 25[4] (2002) 8.
82. S. Orłowska, A. Beroual, and J. Fleszynski, *J. Phys. D: Appl. Phys.* 35 (2002) 2656-2660.